PROBING THE ATMOSPHERE WITH HIGH POWER, HIGH RESOLUTION RADARS

Kenneth R. Hardy
Air Force Cambridge Research Laboratories

and

Isadore Katz
Applied Physics Laboratory
The Johns Hopkins University

ABSTRACT

Observations of radar echoes from the clear atmosphere are presented and the scattering mechanisms responsible for the two basic types of clear-air echoes are discussed. The commonly observed dot echo originates from a point in space and usually shows little variation in echo intensity over periods of about 0.1 second. The results of the most recent investigations of these clear-air dot targets are consistent with the conclusion that most, if not all, of the dot echoes are caused by insects or birds.

The second type of clear-air radar echo appears diffuse in space, and signal intensities vary considerably over periods of less than 0.1 second. The echoes often occur in thin horizontal layers or as boundaries of convective activity; these are characterized by sharp gradients of refractive index. The reflectivity-wavelength dependence of these echoes is consistent with the theory of scattering by fluctuations in refractive index, and the signal intensities can be accounted for by the spectral characteristics of refractive-index variations observed directly.

Some features of clear-air atmospheric structures as observed with radar are presented. These structures include thin stable inversions, convective thermals, Bénard convection cells, breaking gravity waves, and high tropospheric layers which are sufficiently turbulent to affect aircraft.

PROBING THE ATMOSPHERE WITH HIGH POWER, HIGH RESOLUTION RADARS

1. INTRODUCTION

Radar echoes from a clear atmosphere, usually called "angels," have existed almost from the time that radar was first used. Many and varied are the reports in the literature of angel phenomena, and there have been numerous attempts to arrive at a plausible and satisfactory explanation of their origin. A fairly complete background of the entire angel problem is presented in the reviews by Plank (1956), Atlas (1959), Atlas (1964), and Atlas and Hardy (1966). If the vast amount of work reported in these papers were to be summarized as briefly as possible, that summary would indicate that there are just two types of radar echoes from the clear atmosphere (excluding the effects of anomalous propagation). One type appears to originate from a dot or point target whereas the other type extends over a region of considerable horizontal extent. The objective of this paper is to summarize some of the key properties of the two types of clear-air echoes and to present the results of several recent radar investigations of the clear-air echo patterns as observed with three ultra-sensitive radars at Wallops Island, Virginia. Although these radars may be fruitfully used to investigate clouds and precipitation (especially during the early stages of their development), their primary utility is for the observation of the clear-air. Thus, we will restrict the present discussion to clear-air structures.

2. THEORY

The scattering of electromagnetic waves by a turbulent medium has been studied extensively by various investigators (e.g., Booker and Gordon, 1950; Villars and Weisskopf, 1954; Tatarski, 1961). Since clear-air echoes have been observed from regions of the atmosphere where the variations in refractive-index are large, it is useful to state briefly some of the theoretical results which have been obtained. Thus, Tatarski (1961) has derived the expression:

$$\eta = 0.39\, C_n^2\, \lambda^{-1/3} \tag{1}$$

where η is the radar reflectivity, C_n^2 is a measure of the intensity of the refractivity fluctuations, and λ is the radar wavelength. Tatarski also derives the expression

$$C_n^2 = a^2\, L_o^{4/3}\, \overline{(dn/dz)}^2 \tag{2}$$

where a^2 is a nondimensional proportionality parameter, L_o the outer scale or eddy size which defines the outer limit of the inertial subrange of turbulence, and $\overline{(dn/dz)}$ the mean vertical gradient of potential refractive index.

Saxton, et al., (1964) used the same theory as described by Tatarski to derive an expression for the radar reflectivity in terms of $F_n(k)$, the one dimensional normalized spectral density of the mean-square fluctuations of refractivity, $< (\Delta n)^2 >$. Their equation is

$$\eta = \frac{\pi}{8} < (\Delta n)^2 > k^2\, F_n(k) \tag{3}$$

where k is wavenumber and is related to the radar wavelength (λ) by $k = 4\pi/\lambda$. Lane (1967) has pointed out that Eq. 3 is a particularly useful form because

the reflectivity can be evaluated from direct estimates of $< (\Delta n)^2 > F_n(k)$ which are derived from spectral analysis of the field of refractive index. This direct estimate of reflectivity can then be compared to the reflectivity measured with a radar as we will do in Section 5.

Atlas, et al., (1966) give an equation

$$L_o = (\epsilon/\beta^3)^{1/2} \tag{4}$$

where β is the vertical gradient of the mean horizontal wind and ϵ the rate of energy dissipation. The quantity ϵ is an indicator of turbulence because energy dissipation at high rates is accomplished by increased turbulence.

Combining Eqs. (2) and (4) and substituting into Eq. (1), we find that

$$\eta = 0.39\ a^2\ \epsilon^{2/3}\ \beta^{-2}\ (\overline{dn/dz})^2\ \lambda^{-1/3} \tag{5}$$

Equation (5) shows that, if the mean gradients of horizontal wind and potential refractivity are known, an estimate of the turbulence intensity can be obtained by evaluating ϵ from measurements of the reflectivity, η.

Finally, if there are particles in the atmosphere which are small relative to the radar wavelength, then the reflectivity is given by

$$\eta = \pi^5\ |K|^2\ \ \lambda^{-4}\ \Sigma\ D^6 \tag{6}$$

where K is related to the complex index of refraction of the particle, D is the particle diameter, and the sum is taken over a unit volume. Equation (6) is the Rayleigh approximation; it can be applied with very small errors for clouds and raindrops when radar wavelengths greater than 3 cm are used. Comparing Eqs. (1) and (6), one sees that particle scatter can be distinguished from scatter due to variations in refractive index by measuring the reflectivity at more than one radar wavelength.

3. TYPES OF CLEAR-AIR RADAR ECHOES

A multiwavelength radar facility at Wallops Island has been used since 1965 to investigate the nature of clear-air radar echoes. Characteristics of the radars have been tabulated by Hardy, et al., (1966). Briefly, the wavelengths of the radars are 3.2, 10.7, and 71.5 cm, and the minimum detectable cross-section at a range of 10 km is approximately 6.0×10^{-4}, 2.5×10^{-5}, and 3.4×10^{-5} cm^2, respectively.

TABLE 1 illustrates how the Wallops Island radars can readily identify scatterers which are small relative to the wavelength (Rayleigh scatterers) or the scattering expected from refractive index variations. If the pulse volumes are filled with Rayleigh scatterers, then the signal at 3.2-cm wavelength will be about 5 db greater than at 10.7 cm and 30 db greater than at 71.5 cm. On the other hand, if the reflectivity of the scattering medium has a wavelength dependence of approximately $\lambda^{-1/3}$, as appears likely from observations of the clear atmosphere reported by Hardy, et al., (1966) and Atlas, et al., (1966a), then the 3.2-cm signal will be about 15 db lower than

TABLE 1

Ratios of Signal Strengths Expected from Two Types of Scatterers Applicable Only for the Wallops Island Radars

Wavelength (cm)	Ratio of 3.2-cm received power above minimum detectable to that at 10.7 and 71.5 cm (db)	
	Rayleigh scatterers (λ^{-4} dependence)	Scattering from refractive index fluctuations ($\lambda^{-1/3}$ dependence)
3.2	0	0
10.7	5	-15
71.5	30	-20

at 10.7 cm and 20 db lower than at 71.5 cm. Thus, if the signal is stronger at the longer wavelength, it is certain that the mechanism giving rise to the radar echoes is not scattering by Rayleigh particles. The data which follow are interpreted qualitatively with the aid of TABLE 1.

Figure 1 shows simultaneous photographs of the range height indicators (RHI) of the three Wallops Island radars, taken while the beams were scanning synchronously in elevation angle. Except for an overcast cirrus layer, the sky was clear at the time of this observation. The cirrus cloud appears between a height of 7 and 10 km; it is easily identified as it is strongest at 3.2-cm wavelength (top photo), weaker at 10.7-cm wavelength (middle photo), and not visible at 71.5-cm wavelength (bottom photo). Such a drop-off in signal strength with wavelength is expected for Rayleigh scatterers as indicated in TABLE 1. The fact that the numerous dot echoes, appearing between 1 and 3 km in height, are seen most prominently with the 3.2-cm radar and not at all with the 71.5-cm radar indicates that the targets are small relative to the radar wavelength. This observation on the dot echoes, as well as many other types of measurement (for example, the tracking by radar of single known insect species), has led to the conclusion that most of the dot targets are insects (Glover and Hardy, 1966; Glover, et al., 1966).

In Figure 1, the thin layers seen near the surface and at 1 km with the two longer wavelength radars are not attributed to particle scatter. If this were so, the layers would appear much stronger at the shorter wavelength (TABLE 1). Instead, the layers are caused by backscatter from variations in refractive index (Hardy, et al., 1966). These authors show that the wavelength dependence of the echo layers is consistent with the theory of scatter by refractive-index variations [Eq. (1)]. In addition, it has been confirmed that these clear-air radar layers are associated with increased refractivity fluctuations as measured directly with refractometers mounted on aircraft or suspended below a helicopter (Konrad and Randall, 1966).

Another pattern of echo formation is generally found under conditions of

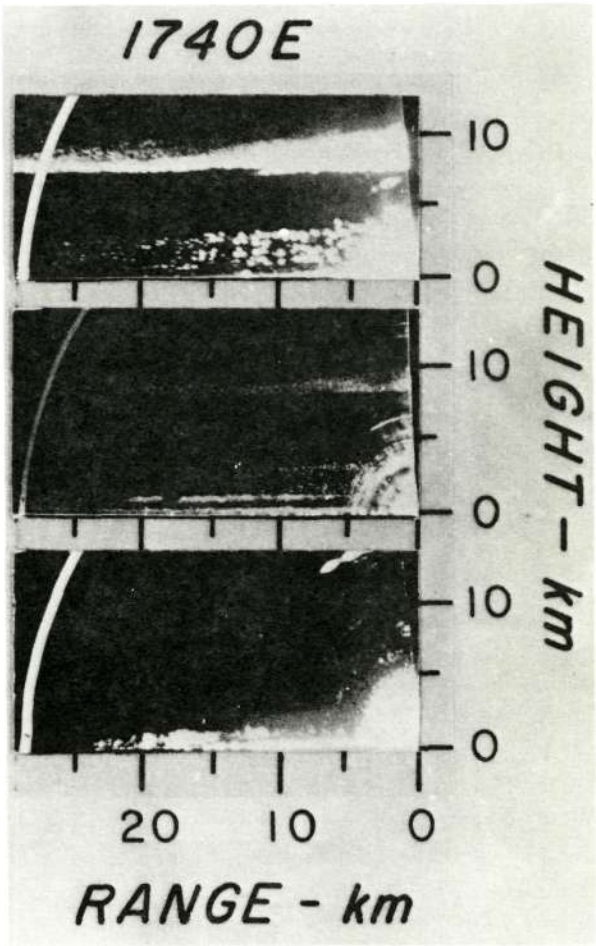

Fig. 1 Photographs of range-height indicators (RHI). The photographs were taken at 3.2-, 10.7-, and 71.5-cm wavelengths (top to bottom) along an azimuth of 260 deg. for 1740 E.S.T. 3 Sept 1966 at Wallops Island, Virginia. The cirrus cloud appears at the shorter wavelengths, whereas the longer wavelength detects only the clear-air variations in refractive index. The numerous dot echoes which appear uniformly distributed between 1 and 3 km at the two shorter wavelengths are due to single insects.

surface heating, both over land and over water. This pattern along with other clear-air structures will be discussed in the following sections.

4. DOT ANGELS

Dot or point angels, as their name implies, appear as point targets on a PPI or RHI scope photograph (Fig. 1). They are also very commonly observed with a fixed vertically-pointing radar beam. An example of dot angels as observed with a 0.86 cm TPQ-11 vertically-pointing radar is shown in Fig. 2. This time-height record was obtained by intensity modulating a scope which was photographed while the film moved continuously at a slow rate. Because of the way the TPQ-11 signal is recorded (Petrocchi and Paulsen, 1966), each dot target appears as a short vertical line. The full vertical lines are at 5-minute intervals and the horizontal dashes correspond to 5000-foot height markers. The lower 3000 to 4000 feet appears filled with dot angels, particularly in the lower half of the figure. In addition, however, there is a distinct tendency for the dot angels to concentrate near heights of 6500 and 8000 feet. The tendency for preferred heights has also been noted by Plank (1956) and Hardy, et al., (1966).

Prior to 1962, there was little known about the wavelength dependence of the

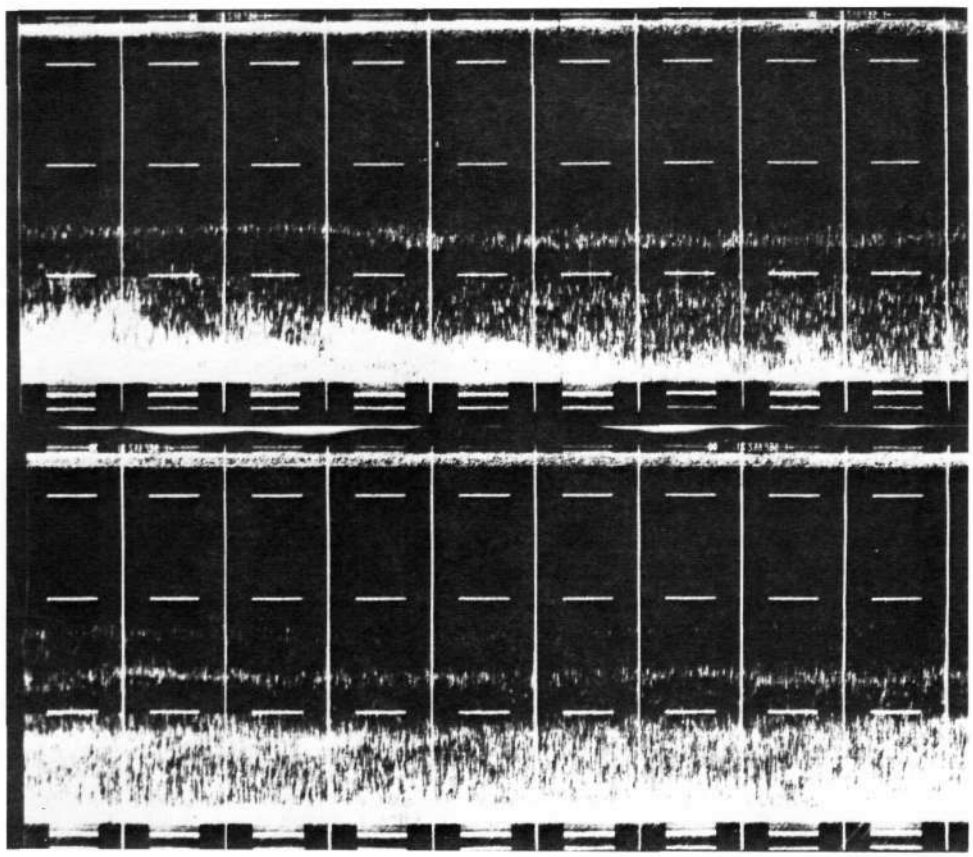

Fig. 2 Dot angels as seen with a vertically-pointing 0.86-cm TPQ-11 radar at Bedford, Mass., 1 Sept 1966, about 1600 E.S.T. The full vertical lines are at 5-min. intervals and the horizontal dashes correspond to 5000-foot height markers. (Courtesy Messrs. Wilbur H. Paulsen and Pio J. Petrocchi, Air Force Cambridge Research Laboratories, Bedford, Mass.)

radar backscattering cross-section of the dot angels. Certainly, dot angels were seen consistently with radars having wavelengths of less than 3 cm (Crawford, 1949; Plank, 1956; Vrana, 1961). However, at wavelengths of about 10 cm, only the recent more sensitive radars were able to detect the relatively small cross-section of the vast majority of dot angels.

Let us look at some of the observations of dot-angel cross-sections as reported by various investigators. These are indicated in Fig. 3. The data by Borchardt (1962), Roelofs (1963), and Fehlhaber and Grosskopf (1964) show cross-sections which range from about 5×10^{-4} to 10 cm^2. The cross-sections reported by Vrana (1961) and Plank (1956) vary from 2×10^{-5} to 8×10^{-2} cm^2. Note that the minimum detectable cross-section of the TPQ-11 radar at a range of 1 km is almost 20 db less than the cross-section of a 1-mm diameter water drop. This radar could detect a single mosquito with ease at ranges of more than 2 km. The cross-sections of Hay and Reid (1962) cover a very large range of values. They use a particularly sensitive vertically pointing radar. But

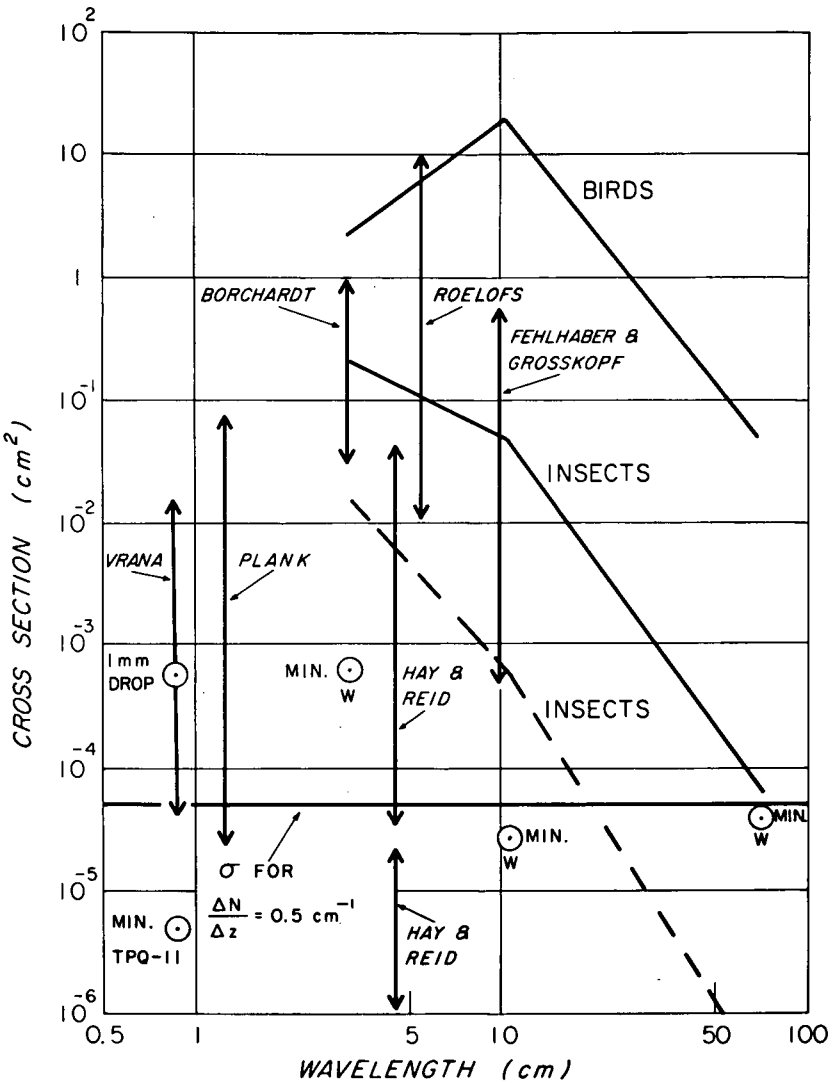

Fig. 3 Cross-sections of dot angels, insects and birds as a function of wavelength. The insect and bird cross-sections are illustrated schematically. The minimum detectable cross-sections for the TPQ-11 radar and the Wallops Island radars are indicated by min. TPQ-11 and min. W respectively.

a vertically pointing radar is not capable of estimating the true cross-section of the target, because it is impossible to know where the target is relative to the beam axis. Thus, a large target near the fringes of the beam would have a small measured cross-section.

The results of cross-section measurements of insects and birds at various wavelengths are indicated schematically in Fig. 3. The curve for birds was chosen as a result of observations at three wavelengths on known birds as reported by Konrad and Hicks (1966) and of additional information presented by Glover and Hardy (1966). There is naturally a large variation in bird cross-sections. Even for the same bird, the cross-section can change by as much as ± 10 db especially at the shorter wavelengths. The general shape of the bird-curve, however, is believed to be quite representative for a large class of birds. The peak in the curve near 10-cm wavelength is probably due to the complicated wavelength dependence which is exhibited by Mie-type scatterers (i.e., the

particle size is of the same order as that of the radar wavelength).

The curves for known insects were similarly obtained from multiwavelength measurements using the Wallops Island radars (Glover, et al., 1966; Glover and Hardy, 1966). The two curves indicate a probable range of values for fairly large insects (maximum size equivalent to a worker honey bee). The cross-sections of insects having dimensions of less than 3 mm are generally undetectable with the Wallops Island radars. The insect cross-sections vary by about ± 5 db at wavelengths greater than 3 cm. There are no extensive cross-section measurements of known insects at wavelengths less than 3 cm. Nevertheless, the cross-sections of water spheres, which have volumes corresponding to those of a large class of insects, fall within the range of 10^{-4} to 10^{-1} cm^2 at wavelengths from 1-3 cm.

The data in Fig. 3 indicate that, taking into account the method of observation, all the cross-section measurements of dot angels fall within the range of values expected for insects or birds. Moreover, based on simultaneous multiwavelength measurements, Hardy, et. al.,(1966), Glover, et al., (1966), and Glover and Hardy (1966) have concluded that all of the dot angels observed in detail have characteristics which identify them as either insects or birds.

An alternative, but unsubstantiated, explanation for dot angels is that they are due to reflections from smooth pseudo-horizontal surfaces across which a large change in refractivity occurs. Atlas (1960, 1964, 1965) and Atlas and Hardy (1966) have described some of the clear-air atmospheric structures which would be required to explain the magnitude of the observed cross-sections. Assuming a refractivity gradient of 0.5×10^{-6} cm^{-1} exists over a smooth surface which was smaller than the first Fresnel zone, then this surface would have a cross-section in the order of 10^{-4} cm^2. The power reflection coefficient of such a surface was assumed to vary as the square of the radar wavelength. From Fig. 3 we see that 10^{-4} cm^2 is near the lower limit of the observed cross-sections of dot angels. This is in spite of the rather optimistic atmospheric structure which was assumed. Atlas (1965) has pointed out that curvature of a surface may result in considerable enhancement of the cross-section. This enhancement would apply to all wavelengths. However, the cross-sections of all dot angels observed at Wallops Island have been strongest at the shortest wavelengths (3.2 and 10.7 cm). Therefore, from the multiwavelength measurements at Wallops Island, there is no evidence of dot angels that are due to atmospheric reflections from sharp refractive-index gradients.

Chernikov (1966) has described some bistatic and depolarization investigations of dot angels. Contrary to his preliminary results, Chernikov (1966) now states that the experiments carried out provide convincing evidence that the overwhelming majority of dot-angel echo targets are insects and other particles introduced into the atmosphere. Fehlhaber and Grosskopf* have arrived at the same conclusion after a reexamination of their bistatic measurements on dot angels. In summary, it would appear that insects or birds can account for the vast amount of observational radar-data on dot angels.

* Private communication

5. CLEAR-AIR ECHOES OF HORIZONTAL EXTENT

5.1 General Features

Atlas (1964) has reviewed some of the early results of radar echoes from stratified layers. These layers usually corresponded in height to regions having sharp vertical gradients in refractive index. Additional evidence for the existence of clear-air radar layers associated with large variations of refractive index is given by Saxton, et al., (1964), Ottersten (1964), and Hardy, et al., (1966).

Fig. 4 is an example of uniform, stratified layers as they appear on RHI photographs. These data were obtained with the 10.7-cm radar at Wallops Island at 0530 EST while the sky was perfectly clear. The layer near 1 km appears at all three azimuths and is coincident with a very pronounced inversion (Hardy and Glover, 1966). It is typical of the type of layer observed in the vicinity of very stable layers, but yet the variations of refractive index within the layer may be large (Lane, 1964).

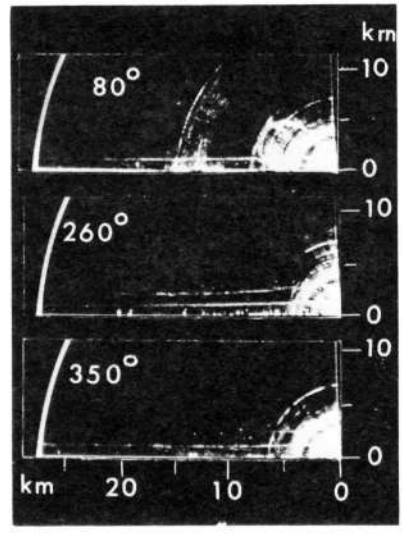

Fig. 4 Photographs at three azimuths of the range-height indicators at a wavelength of 10.7 cm at Wallops Island, Va., 0530 E.S.T., 4 Sept 1965. The sky was perfectly clear at the time of the observation. The layer near 1 km is coincident with a very pronounced inversion. The circumferential arcs at short ranges are ground echoes seen by the side lobes. (From Hardy and Glover, 1966.)

The variation of the reflectivity of clear-air layers as a function of wavelength is shown schematically in Fig. 5. Some typical values of reflectivity observed with the Wallops Island 10.7 and 71.5-cm radars are indicated in the right-center of the figure. The slopes of the lines are close to the 1/3 power as expected for scatter from refractive index fluctuations (Eq. (1)), but in practice there is considerable variation in this slope for individual measurements. For comparison, the reflectivity-wavelength relationship observed in a particularly dense layer of insects (concentration of about 5×10^{-6} m^{-3}) is also indicated. It is evident that the two types of scatterers can be readily identified on the basis of their wavelength dependence (see also Fig. 1). Also indicated in Fig. 5 are the approximate maximum values of the 10-cm radar reflectivity as observed by Ottersten (1964) and by the Wallops Island 10.7-cm radar in regions which apparently were not contaminated with any insects.

Values of the coefficient C_n^2 derived from Eq. (1) are shown on the scale at the right. The C_n^2 values of the clear-air radar layers are usually in the range of 10^{-15} - 10^{-14} $cm^{-2/3}$, but maximum values as high as 10^{-12} $cm^{-2/3}$ may occur on rare occasions.

C.5

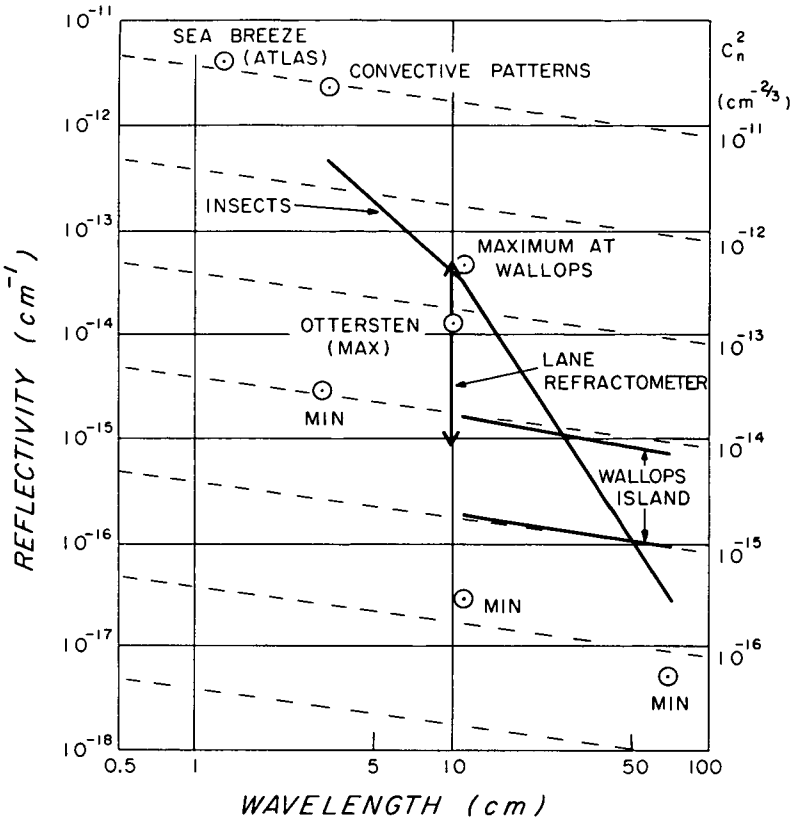

Fig. 5 Radar reflectivity as a function of wavelength for clear-air radar echoes. The values of the three-dimensional fluctuations in refractive index, C_n^2, as derived from theory are shown on the scale at the right. The reflectivity varies approximately as wavelength to the -1/3 power for scattering from refractive-index fluctuations and wavelength to the -4 power for insects. Values of reflectivity derived from direct measurements of refractivity spectra are consistent with the reflectivities observed with radar.

Balloon-borne refractometer soundings, carried out by Lane (1967) in England, have shown that at or near the base of elevated inversions and isothermal layers there are eddies within which unusually large values of variance $\langle(\Delta n)^2\rangle$ are observed. Lane has performed a spectral analysis of 20 records, all of which were taken in layers which correlated with vertical-incidence 10-cm radar echoes. He then extrapolated values of $\langle(\Delta n)^2\rangle F_n(k)$ corresponding to a radar wavelength of 10 cm ($k = 4\pi/\lambda = 1.25$ cm^{-1}). From Eq. (3), he was able to estimate the reflectivity due to scattering from observed variations in refractive index. The range of reflectivity values thus computed for

the 20 spectra are indicated by the double-ended arrow at 10-cm wavelength in Fig. 5.

As seen in Fig. 5, the range of reflectivities expected from the direct refractivity measurements in England are in excellent accord with the reflectivities obtained from radar measurements in Sweden and the U.S. (Lane estimates crudely that the reflectivities, observed with the radar used in conjunction with his refractometer soundings, were also consistent with those observed by Ottersten.) Realizing that the data presented in Fig. 5 are subject to errors in the order of several db, it can, nevertheless, be seen that there is gross quantitative agreement between the radar observations and the corresponding direct atmospheric measurements.

There are two additional data points on Fig. 5 which have not been mentioned. These occur at wavelengths of 1.25 and 3.2 cm and correspond to C_n^2 values of about 10^{-11} $cm^{-2/3}$. The 3.2-cm value was estimated from clear-air echoes during a time when insects were bountiful in the layer near the surface (Section 7). The value at 1.25 cm has been estimated from the radar observations of the sea-breeze reported by Atlas (1960a). Although refractive-index variations at a sea-breeze front are likely to be comparable to the maximum values which can exist in the atmosphere, it is difficult to picture more than an order of magnitude increase in C_n^2 at a sea breeze front over the C_n^2 observed in elevated layers. An alternative explanation is that a few insects were within the pulse volume and resulted in a significant contribution to the received signal. This possibility has appeal because of the relative ease at which short wavelength radars detect insects (Fig. 3), and it would obviate the need to explain refractive-index variations of more than an order of magnitude larger than those which have been observed or estimated by other techniques.

5.2 Experiments to Validate Theory

The expression given by Saxton, Eq. (3), states the relationship between radar reflectivity and the spectral density of refractive-index fluctuations. Tests have already been mentioned which have shown a qualitative association between regions of high variance in refractivity and the presence of clear-air echoes. Some experiments were also performed at Wallops Island which were directed toward a quantitative check of this theoretical relationship.

The technique used in these experiments involved tracking the meteorologically-instrumented aircraft with the radar, making radar measurements and meteorological measurements simultaneously. The radar automatically tracked the incoming aircraft with a tracking gate. A "data" gate was slaved to the tracking gate and was positioned just ahead of the aircraft; radar signal strength was measured in that volume of space determined by the data gate and radar beamwidths. The airplane flew into this volume about 10 seconds after the radar had a measure of its reflectivity. By taking this lag into account, one could compare radar reflectivity with the spectrum of the refractivity fluctuations.

Figure 6 shows the results of this experiment. Along the abscissa are values of $\frac{\pi}{8} k^2 \langle(\Delta n)^2\rangle F_n(k)$ and along the ordinate are values of radar reflectivity. The points showing the spectral values on the graph were obtained by

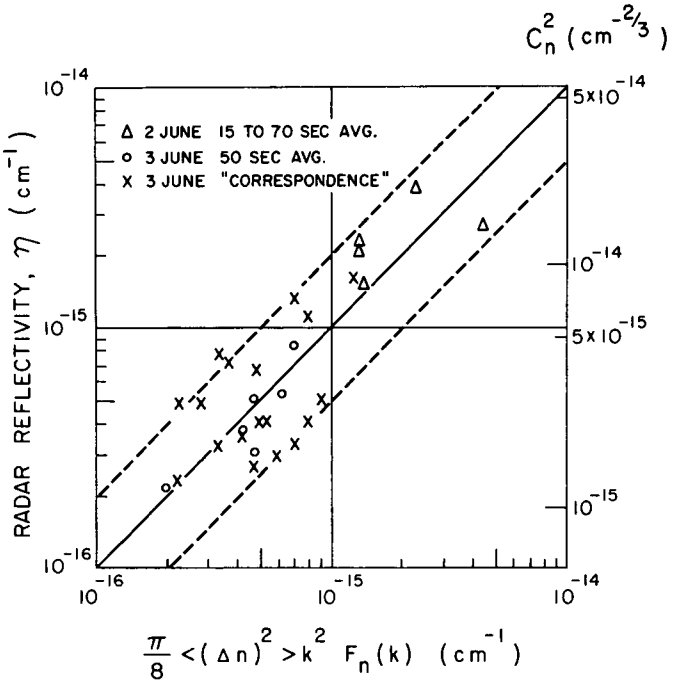

Fig. 6 Radar reflectivity as a function of spectral density or refractive index. Spectral density was obtained by extrapolating computed spectra down to wavenumber, k, corresponding to one-half the 10.7-cm radar wavelength. For almost all cases the radar reflectivity corresponds to within 3 db of that expected from direct refractometer measurements. (From Kropfli et al., 1968.)

extrapolating the measured spectra to the appropriate wave number as was done by Lane (1967); this was necessary because the size of the sampling refractometer cavity precluded making direct measurements of the small atmospheric eddies. The solid line is the relationship expected from Eq. (3). It can be seen that most of the points fall within the 3 db bounds (shown as broken lines). It is possible to draw three conclusions from these results: (1) the "-5/3 law" is applicable to these atmospheric conditions, (2) the microscale cutoff is at a wave number greater than 5 cm, and (3) the theory which leads to Eq. (3) has been confirmed experimentally.

A continuation of this type of fine scale comparison is being planned. Clearly, it would be preferable to avoid extrapolation by measuring fluctuations in refractivity with devices sufficiently small that their frequency response lies in the appropriate region. This is already feasible using hot-wire anemometers and fine-wire thermometers. Rapid progress is being made in small-volume humidiometers and one is being installed for flights during the summer of 1968. To date, however, refractometers are unable to measure the atmosphere with the required resolution. It is strongly suggested that this is an area requiring active and high-priority research.

6. CONVECTIVE THERMALS

During clear days in the summer, convective patterns are observed consistently in the lower atmosphere with the 10.7 cm radar at Wallops Island. These patterns appear as wave-like perturbations on an RHI presentation and are illustrated in Fig. 7. The top photo (X-band, 3.2 cm) shows a few echoes at a height of about 800 m spaced 2-3 km apart. The corresponding echoes are much stronger in the middle photo (S-band, 10.7 cm), and this confirms that the scattering is from variations in refractive index (TABLE 1 and Fig. 1).

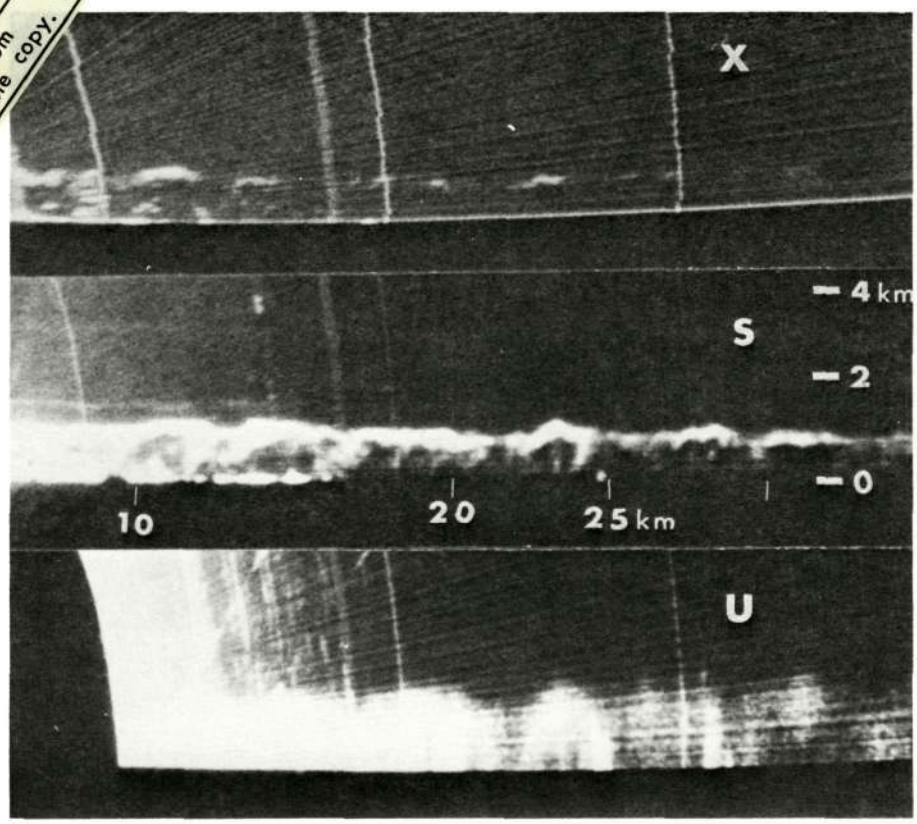

Fig. 7 Simultaneous photographs of range-height indicators at wavelengths of 3.2 cm (X-band), 10.7 cm (S-band), and 71.5 cm (UHF) taken while the sky was clear, 0850 E.S.T., 10 May 1966, at Wallops Island, Virginia; azimuth 250 deg. The definite wave-like perturbations are the boundaries of convective cells (Fig. 8a).

The bottom photo (UHF, 71.5 cm) shows extensive echoes out to a range of more than 30 km. Because of the broad 3-degree beam of the 71.5-cm radar (compared with the 0.5 degree beam of the 10.7-cm radar), the echoes are spread out at the longer wavelength.

The horizontal pattern of the echoes, shown in Fig. 8a, reveals that the echo-structure is actually circular or elliptical having diameters of 1-3 km and echo-free centers. There were cumulus clouds in the area at the time the photo shown in Fig. 8a was taken, and it is probable that many of the echoes are coming from cloudy regions. Nevertheless, the echoes are seen by virtue of scattering from refractive-index variations as established from the multi-wavelength measurements. Furthermore, essentially identical patterns have been observed during a perfectly clear day (Atlas and Hardy, 1966).

Figure 8b is a sketch of the atmospheric structure which might produce the observed echo pattern. It shows a rising plume of air or thermal. The sketch was derived not only from the data shown in Figs. 7 and 8a, but was also derived from a series of PPI photographs taken at successively increased ele-

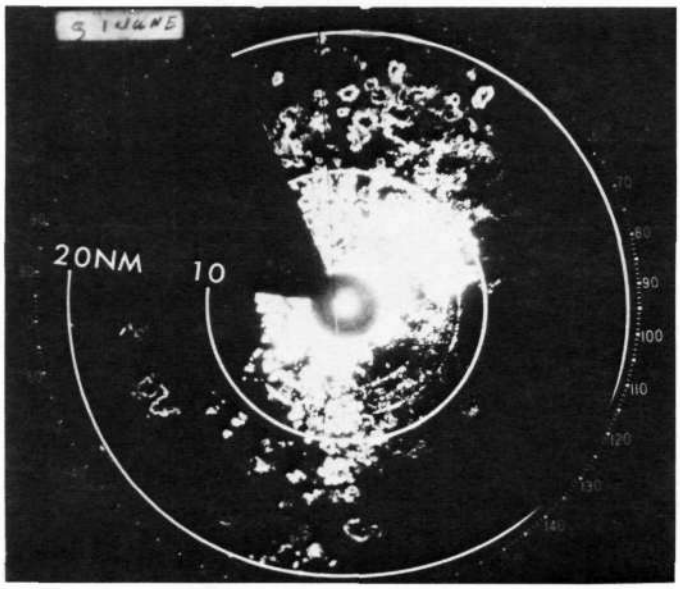

Fig. 8a Photograph of sector plan-position-indicator (PPI) at wavelength of 10.7 cm with 12 db attenuation; 1023 E.S.T., 1 June 1966, at Wallops Island, Virginia, elevation 5 deg., and range marks are at 10 n. mi. (18.5 km). Some of the intense echoes within 10 n.mi. are due to ground clutter. The radar beam cuts through the convective cells seen in Figure 7 showing that the cells are circular or elliptical with echo-free centers.

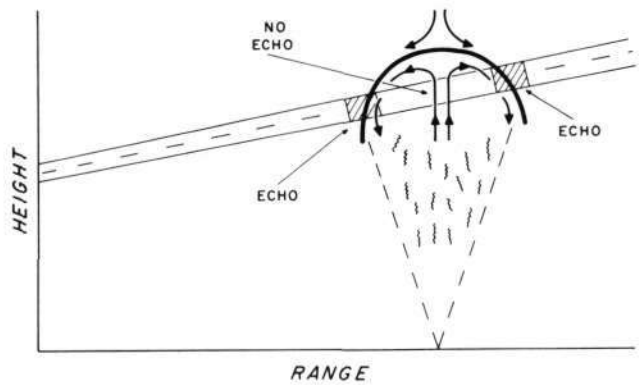

Fig. 8b Sketch of convective cell showing the refractivity structure which results in the observed doughnut-like echoes.

vation angles. These photos indicated that the hole regions became progressively more echo filled at greater heights in the atmosphere, and that the overall diameter of the echoes also diminished. The sketch indicates that the flow within the convective cell is upward in the center and that the relative flow around the periphery is downward. This model would be expected to give the maximum gradients of refractive index near the top of the cell, decreased gradients around the periphery, and relatively small gradients in the cell center where the air was fairly uniform.

7. BÉNARD-LIKE CONVECTION CELLS

The convective patterns described in the previous section had diameters in the order of 1-3 km, probably updrafts in their center, and were due to scattering from refractive index variations. In this section a different type of convective pattern is described.

Figure 9 is a photograph of a PPI of a CPS-9 (3.2 cm) radar taken at 0 degree elevation on 23 May 1966 at Sudbury, Massachusetts. Except for a few fair weather cumulus clouds (< 1/10 coverage) the sky was clear at the time of

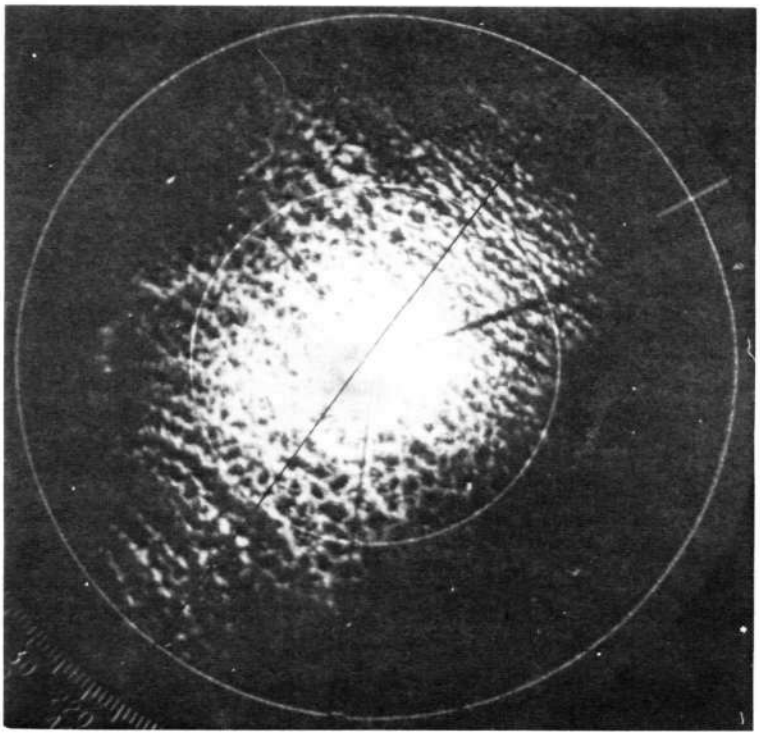

Fig. 9 PPI photo at 0 deg. elevation angle taken at 1120 E.S.T. on 23 May 1966 while the sky was essentially clear. The major range marks are at 25 n. mi. intervals. The radar is a 3.2-cm CPS-9 located at Sudbury, Massachusetts. A mesoscale cellular pattern, similar to the Bénard circulation patterns studied extensively in the laboratory can be seen. The individual cell has a diameter which varies from 5-10 km, a lifetime of at least 30 minutes, and is made up of several smaller cells. The echoes are due to scattering from insects which occurred in abnormally high concentrations during the observations. The insects apparently provide excellent tracers of the mesoscale atmospheric circulation.

the observation. A cellular pattern, similar to the Bénard Circulation patterns studied extensively in the laboratory (Brunt, 1951), is clearly evident. The diameters of the cells vary from 5-10 km and are similar to those discussed by Atlas (1959a). In contrast to the pattern shown in Fig. 7, an RHI of the Bénard-like echoes showed that the strongest reflectivities occurred near the surface. Furthermore, the boundary of each cell in Fig. 9 was composed of a series of intense cores spaced about 5 km apart and extending upward to a height of about 2 km. A study of the Bénard-like cells revealed that the flow pattern probably was slowly upward around the periphery of the cell and downward in the center. Superimposed on the upward peripheral motion were cores of more intense updrafts which had dimensions of, and resembled, the smaller convective thermals seen in Figs. 7 and 8a.

It is of interest to consider the source responsible for the clear-air

echoes evident in Fig. 9. It is estimated that their reflectivity is 15 db larger than the maximum clear-air reflectivity observed with the 3.2-cm radar at Wallops Island. This is illustrated in Fig. 5 which shows the reflectivity of the convective patterns to be considerably larger than the maximum clear-air reflectivity observed or estimated by other investigators. Because of this incredibly large reflectivity, it is not considered possible that the scattering is from variations in refractive index.

The only other echo source that might account for the Fig. 9 echoes is particulate matter and insects (Hardy, et al., 1966). To obtain a 3.2-cm reflectivity of 3.2×10^{-12} cm^{-1} as observed (Fig. 5), insects would have had to be present which had a radar cross-section equivalent to that of a 0.5-cm diameter water sphere and which had a number concentration of about 3×10^{4} km^{-3}. If the insects were smaller, of 0.25-cm water sphere equivalent, then the required concentration would have been about 3×10^{6} km^{-3}. The latter concentration, in more reasonable units, is equivalent to 3 insects per cube having sides of 10 m length. This concentration is approximately equivalent to one insect per 20 people on a crowded beach! Insects the size of a small house fly or a flying ant have cross-sections in the 0.25 - 0.5-cm water sphere category (Hajovsky, et al., 1966). Of particular interest is the fact that, during the time the Fig. 9 patterns were observed, there was an abnormally large number of flying ants and other insects in the vicinity of the radar site. At the particular season of the year (May), it is common for a variety of insects to swarm. Thus it appears that insects were mainly responsible for the echoes shown in Fig. 9 and that, on occasion, the insects provide an excellent source of tracers for atmospheric flow circulations.

8. BREAKING GRAVITY WAVES

Hicks and Angell (1968) have investigated an apparent horizontally twisted or braided atmospheric structure which frequently appears in the RHI photographs. An example of such a braided structure, occurring at a height of 3.5 km (11,500 ft.) in a clear atmosphere, is shown in Fig. 10. The most reflecting portions of this echo structure slope upwards from right to left. That is, the echo strengths are not uniform along a single filament. Two filaments, however, combine to give the appearance of a braid.

During a six-week observational period in May and June, 1966, there were eleven occurrences of braided structures. The braided appearance persisted for at least several minutes, although adequate data to determine the actual lifetime of the phenomenon were never obtained. Since the braided appearance could be identified over a fairly large horizontal region, the rather obvious explanation that it is due to the intertwining of two filaments of increased refractivity must be ruled out. Other important features of this structure are that it shows a preference to be aligned in the direction of the wind shear, and it occurs in regions of relatively stable lapse rates or inversions. These environmental conditions are favorable to the formation, development, and breakdown of gravitational waves (Haurwitz, 1941), and the breakdown of gravitational waves is the explanation arrived at by Hicks and Angell.

The braided structure is sometimes preceded by the presence of stable waves which gives additional support to the breaking-wave explanation. Figure 11

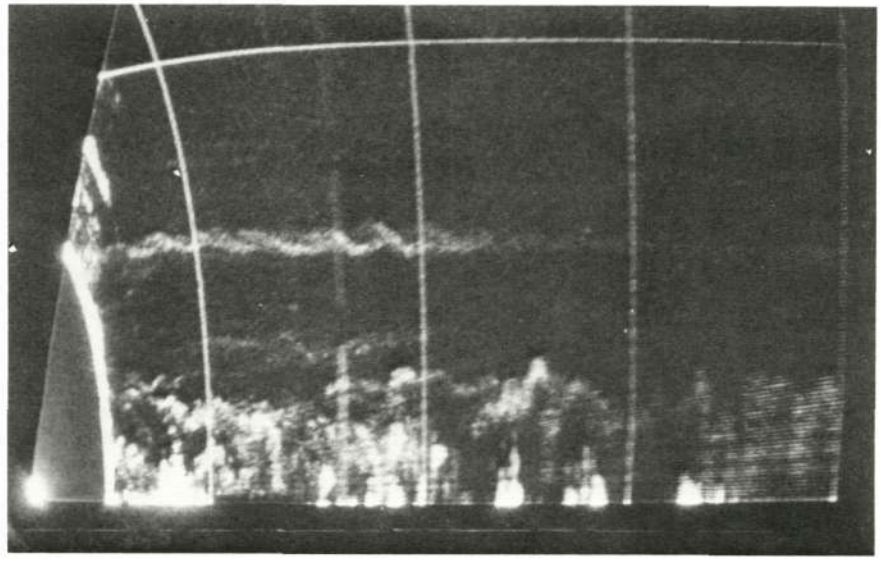

Fig. 10 Photograph of RHI scope of the 10.7-cm radar at Wallops Island taken on 1 June 1966, 1432 E.S.T., with 9 db attenuation, showing a twisted or braided structure near 11,500 ft. The height mark is near 20,000 ft. and the range marks are at 5 n.mi. intervals. The echoes below about 6,000 ft. are from cloudy regions, but the region near 11,500 ft. is probably clear. (From Hicks and Angell, 1968.)

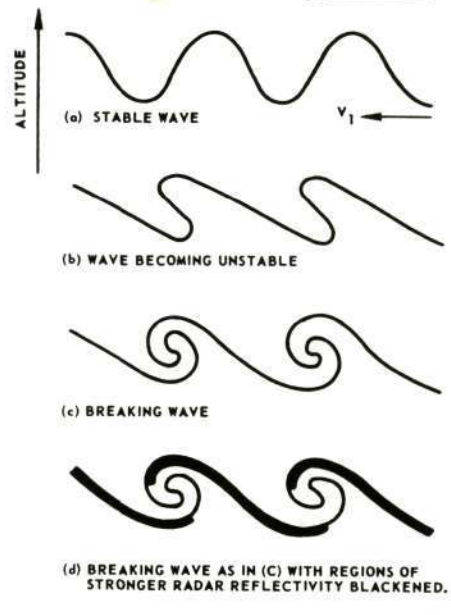

Fig. 11 Sketch of gravitational wave embedded within a layer with winds increasing with height: (a) wave stable, (b) wave becoming unstable, (c) wave breaking and forming vortices (Fig. 12), and (d) same as (c) except with regions of stronger radar reflectivity blackened. (From Hicks and Angell, 1968.)

shows how breaking gravity waves, in cloudless regions, may give the appearance of braided structures when viewed with a radar. Figure 11a is a sketch of a stable gravity wave embedded in a layer having a velocity shear in the vertical,

11b depicts the wave becoming unstable, and 11c shows the wave breaking with the resultant forming of vortices. Figure 11d is the same as Fig. 11c, but now the solid portions of the breaking wave represent the stronger radar reflectivity and the lighter portions the weaker. This illustrates how a breaking gravity wave may actually appear as a braided structure on radar and yet is consistent with the observation of discontinuities which were evident in one of the braids.

Essentially the same structure seen by radar in a clear atmosphere is occasionally observed visually in cloud formations as the remarkable photograph of Fig. 12 illustrates. This picture was taken in Colorado, and the breaking waves are seen by virtue of the cloud droplets which provide excellent tracers for the air flow. Figure 12 is essentially identical to the structure depicted in Fig. 11c, and provides virtually irrefutable evidence that the mechanism proposed by Hicks and Angell for the braided radar structure is correct.

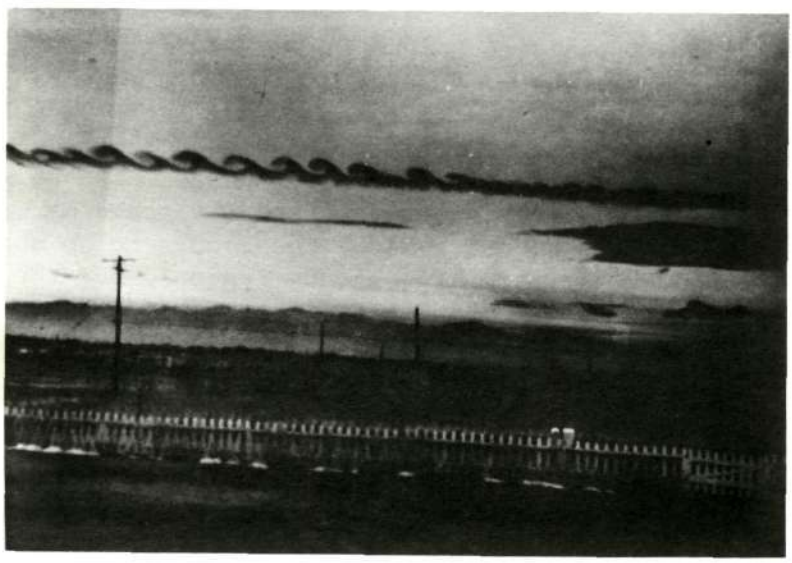

Fig. 12 Breaking gravitational waves seen visually by virtue of clouds defining the flow pattern. Note the similarity with the radar braided structure shown in Fig. 10. (Photo courtesy Mr. Paul E. Branstine. See Colson, D., 1954: Weatherwise, 34-35.)

9. CLEAR-AIR TURBULENCE

Usually the strongest clear-air radar echoes occur in the lower 3 to 4 km of the atmosphere. Such a result is expected from Eq. (5) because the very large mean gradients of refractive index are possible only in the lower few kilometers; that is, significant moisture gradients occur only in the lower troposphere and the refractive index is most sensitive to moisture. Moreover, the lower clear-air layers are usually not turbulent, at least not on the scale that affects aircraft. This has been confirmed by numerous aircraft flights in the lower 4 km made in conjunction with the radar observations at Wallops Island. Therefore, it is probable that, in the lower troposphere, the gradient of refractive index is usually the dominant factor determining

whether or not a clear-air layer will be detectable.

In spite of the predominance of clear-air radar layers in the lower troposphere, the layers of main concern in this section are those that occur in the upper troposphere or above approximately 6 km. Figure 13 shows one of these layers. It occurs at a height of 12 km out to a range of at least 30 km. From multiwavelength measurements it was determined that this layer was caused by scattering from refractive-index variations (Atlas et. al., 1966 b). The layer from about 7 to 10 km in altitude is cirrus cloud.

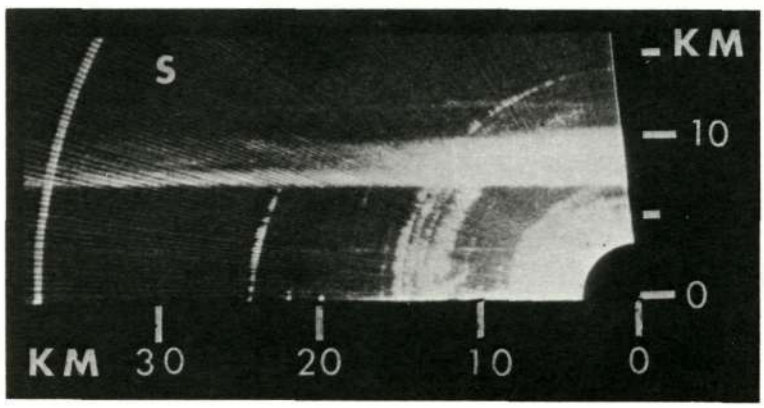

Fig. 13 Photograph of RHI at wavelength of 10.7 cm, 1030 E.S.T., 18 February 1966, at Wallops Island, Virginia, azimuth, 90 deg. The strong echo between 7 and 10 km is due to scattering from cirrostratus clouds. The echo layer near 12 km height occurs in a clear region and is associated with the tropopause. (From Atlas et al., 1966b.)

The tropopause, at the time of the observation shown in Fig. 13, was at essentially the same height as the 12 km radar layer. Tropopause layers and clear-air layers above 6 km have been observed on numerous occasions during the winter months of 1966-67. A particularly interesting tropopause layer is shown in Fig. 14. Waves of fairly low amplitude are clearly evident within this layer. These non-breaking gravity waves at the tropopause level have been observed on one additional occasion in which the wave amplitude was considerably larger than that shown in Fig. 14. It was inferred by Atlas, et al., (1966a and 1966b) that turbulence sufficiently intense to affect aircraft was necessary before the region at the tropopause level could be detected. This inference is supported by recent experimental results.

Hicks, et al., (1967) have described experiments in which the high-altitude clear-air layers were probed with an uninstrumented F-106 aircraft. While the aircraft performed spiral ascents, descents or horizontal runs at the altitude of interest, the radar scanned in elevation in order to obtain data on all the echo layers within a vertical plane. The pilot reports provided a qualitative estimate of the location and severity of turbulence encountered.

The results of four aircraft flights and the corresponding 10.7-cm radar observations for regions above 6 km are summarized in Fig. 15. Cloud echoes

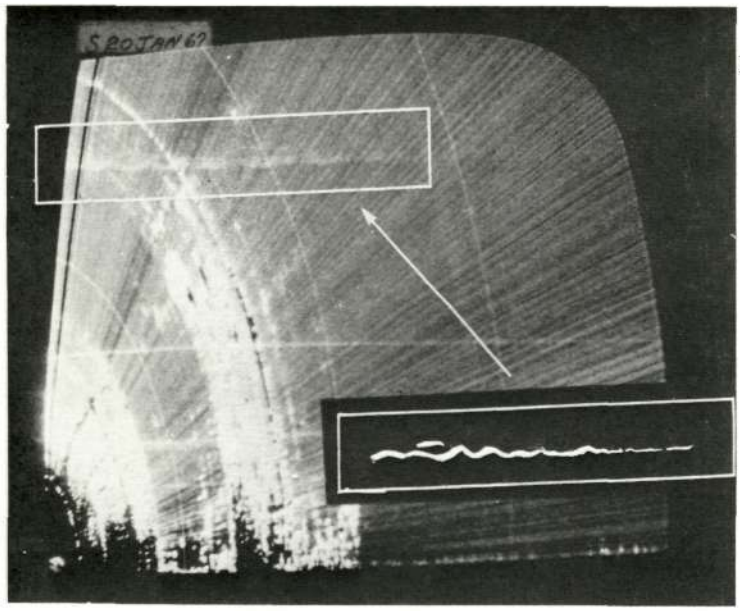

Fig. 14 Photograph of RHI at wavelength of 10.7 cm, 0912 E.S.T., 20 Jan 1967 at Wallops Island, Va., azimuth 70 deg. The range marks are at 5 n. mi. intervals and a height marker occurs at 20,000 ft. The low amplitude waves seen near 39,000 ft. occur in clear air (see inset for tracing of pattern) and are coincident with the height of the tropopause.

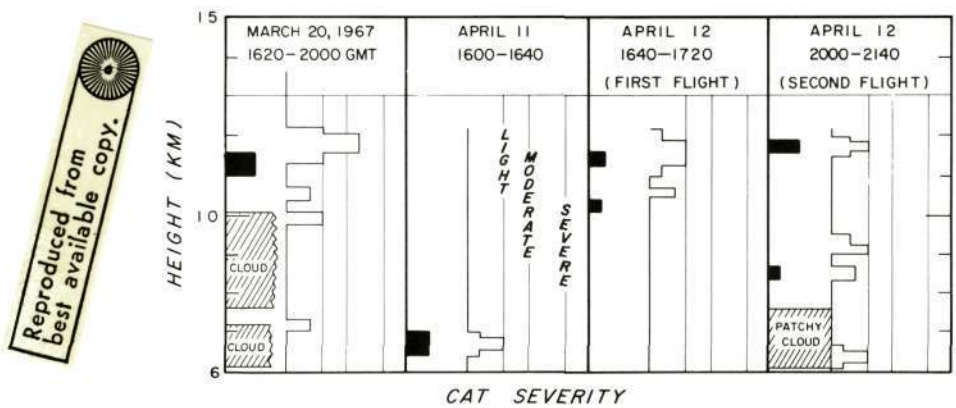

Fig. 15 Heights of radar echoes and reports of clear-air turbulence. Clear-air echoes are indicated by the solid areas, cloud echoes by the hatched areas, and the aircraft encounters with CAT by the open areas. The severity of CAT is indicated by a relative scale deduced from the pilot reports. The horizontal extent of the solid areas is roughly proportional to the radar reflectivity of the clear-air echoes. (From Hicks et al., 1967.)

are indicated by the hatched areas, clear-air echoes by the solid areas, and the aircraft encounters with clear-air turbulence (CAT) by the open areas. The correspondence in altitude between the clear-air radar echoes and the clear-air turbulence encounters is excellent. On all occasions, the regions of clear-air echoes above 6 km which were simultaneously probed with the aircraft were found to be turbulent. This appears to be the first time that aircraft and radar have probed the same region of space and confirmed the close relationship

between the high-altitude clear-air radar echoes and turbulent aircraft flight.

The high-altitude radar echoes were thin (200 to 600 m), stratified, and somewhat patchy (horizontal dimensions in the order of 5 to 15 km). Moreover, the echoes were not particularly persistent, often lasting for less than a few tens of minutes. The CAT was also reported to be in relatively thin layers, the maximum thickness being about 1.5 km centered near a height of 11.5 km during the first flight on 12 April. Although not determined precisely, the lateral extent of CAT was found to vary over narrow horizontal limits, usually less than 30 km. These dimensions are consistent with other aircraft probes of CAT (Reiter and Burns, 1966) emphasizing the patchiness which generally characterizes CAT. This patchiness is evident from both the radar and aircraft probes.

The results in Fig. 15 suggest that ultra-sensitive microwave radars can detect regions of CAT. A limitation, however, is the rather restricted range (less than 30 km) of the present CAT-detection capability. Moreover, as seen in Fig. 15, light CAT not detected with radars is encountered occasionally.

10. METEOROLOGICAL RELEVANCE

Results thus far obtained on the multiwavelength high-power radar system discussed in this paper open vast new possibilities for the meteorologist. He can now investigate atmospheric processes, on scales up to 50 miles, in a 3-dimensional manner and practically instantaneously.

It has been stated previously that clear-air convective patterns are often observed both over land and water. The relationship between this clear-air pattern and subsequent cloud formation and development requires further investigation. A multiwavelength high-resolution ultra-sensitive radar facility provides a unique opportunity for studying clear-air structure, clouds, and precipitation and their interrelationships.

At present, meteorologists make wind velocity measurements by tracking balloons once every six hours. This yields a single wind speed at one point in space at each elevation. Photographs of clear-air radar echoes have shown wind fields in which the direction changes by perhaps 20 degrees within a 20-mile radius of the radar. This might indicate local convergence or divergence, for example. Observations like these may well lead to new methods for predicting cloud formation and dissipation.

By using the Doppler information, one could look for regions of high variance and thus find turbulence. This subject has already been discussed in this paper, but there are other aspects which are of interest. For example, a high-power Doppler radar could be used to determine gustiness over an airport to aid landing operations or in the region of a missile launcher to advise of appropriate meteorological launching conditions. Also, for a properly situated radar, one may well study such local effects as the sea breeze or make substantial contributions to solving the complex problem of air-sea interaction.

One may use remote radar probing techniques to shed light on diffusion processes. Since the radars detect regions of large variance in refractivity,

which implies mixing between two masses of air of originally different properties, it means that eddy diffusion is already in progress when detection takes place. Detection ceases when mixing is complete; homogeneous air does not lead to radar reflections. Thus the progression of the diffusion might well be determinable; more specifically, one may study diffusion coefficients under various conditions of stability.

The above illustrations indicate only a few of the possibilities. One way to summarize is to say that with high-power narrow-beam radars the clear atmosphere has become "visible". Motions and processes in the air, undetectable up to the present time except by single point sensors, are now susceptible to quantitative analysis.

11. FUTURE DEVELOPMENTS

11.1 Forward Scatter

Forward scatter experiments are being discussed in detail at other sessions. However, it should be mentioned here that several forward scatter paths are under consideration in connection with the Wallops Island radar site.

One proposed link is between Wallops Island and Valley Forge, Pennslyvania, a distance of about 250 km. The transmitter will operate at S-band and use a 50-foot precision parabola with ability to scan vertically. The receiving system will be the present S-band radar operated as a receiver only. It is anticipated that the two large antennas (1/2 degree beams) will result in small enough common-volume resolution cells to facilitate identification of the reflecting layers.

The second path under consideration is an X-band link between Wallops Island and Westford, Massachusetts, using a mobile X-band transmitter at Wallops Island (6-foot antenna) and the 60-foot dish at Westford for reception.

One advantage stemming from a combined forward-scatter link and a high-power radar lies in the fact that the radar can identify the altitudes of the reflecting layers if they are within the detection range of the radar. Identification of the positions of the reflecting layers has thwarted interpretation of previous forward-scatter data.

Clearly, one could be more certain of successful interpretation on a forward scatter link by setting one up on a north-south path with the Wallops Island radars at the midpoint. This would assure identification of many high-altitude layers by backscatter radars; the positions of these layers could then be used to interpret the simultaneous forward-scatter signals.

11.2 Information Processing

One aspect which must be given attention is that of information display and utilization. Much can be said about the advantages of Doppler radars, but to date only a small proportion of Doppler data have been used for atmospheric research. The major difficulty lies in interpretation of the data. One can use a velocity-azimuth mode of operation which provides a wind speed at a

selected altitude. However, it has already been pointed out that wind velocity varies in both space and time in the hemisphere surrounding the radar. Although the velocity component toward the radar is measurable in the entire hemisphere and its spectrum (or velocity variance) is obtainable, the amount of information thus obtained is so large as to be unuseable. Methods must be devised to measure, analyze, digest, and put into useable form the 3-dimensional picture of the wind field. Presently available techniques are inadequate.

12. SUMMARY

This review describes some of the recent observations of radar echoes from the clear air with the object of substantiating the conclusions as to their origins and to illustrate how clear-air radar echoes can be used to investigate a wide range of atmospheric structures.

The radar cross-sections of dot angels at wavelengths from 0.86 to 71.5 cm are consistent with the range of cross-sections expected for insects or birds. Similarly, it has been concluded from simultaneous multiwavelength measurements and from recent bistatic depolarization studies that all of the dot angels observed in detail have characteristics which identify them as either insects or birds.

Powerful radars at 10-cm or longer wavelengths regularly detect narrow layers of clear-air echoes which have considerable horizontal extent. These layers correspond in height to regions having sharp vertical gradients in refractive index. The reflectivity-wavelength dependence is consistent with the theory that the scattering occurs from eddies having a spectrum of refractive index which is proportional to the -5/3 power of the eddy wavenumber (Hardy, et al., 1966; Atlas, et al., 1966a). Moreover, excellent agreement has been found between the observed radar reflectivity and the reflectivity computed from the observed fluctuation-spectrum of refractive index. These results indicate, (1) scattering from the clear atmosphere can be described quantitatively in terms of the refractivity spectrum, and (2) the -5/3 refractivity spectrum well represents the atmosphere out to limiting microscales smaller than 5 cm.

Clear-air convective thermals having diameters of 1-3 km are often observed with sensitive 10-cm radars. These thermals are seen by virtue of the scattering from refractive-index fluctuations, and in plan view, they typically appear circular or elliptical and have echo-free centers. It is suggested that the flow within these convective thermals is upward in the center and that the relative flow areound the periphery is downward.

Bénard-like convective cells having diameters in the order of 10 km have also been observed occasionally using a 3.2-cm radar of moderate sensitivity. It is shown that the radar echoes on these occasions are due to an unusually large increase in the number of insects in the atmosphere. The atmospheric flow in these Bénard-like cells is probably upward around the periphery of the cells and downward within their centers.

An apparent horizontally braided atmospheric structure is sometimes

observed in the clear atmosphere with the 10.7-cm radar at Wallops Island. This structure shows a preference to be aligned in the direction of the wind shear, and it occurs in regions of relatively stable lapse rates or inversions. These features and the characteristics of the radar-echo structure have led to the conclusion that the braided appearance is caused by breaking gravity waves. Non-breaking waves have also been observed, and these often occur at the height of the tropopause.

In an effort to determine the degree of turbulence associated with the high-altitude clear-air layers observed with the Wallops Island radars, the regions have been occasionally probed with an aircraft. The pilot-reports provided a qualitative estimate of the location and severity of turbulence encountered. On all occasions, the regions of clear-air echoes above 6 km which were simultaneously probed with the aircraft were found to be turbulent. This experimental result is consistent with the conclusion previously inferred on theoretical grounds that turbulence sufficiently intense to affect aircraft appeared necessary before the regions of turbulence in the upper troposphere were detectable.

14. ACKNOWLEDGMENTS

The research conducted at Wallops Island, Virginia, has been supported in part by the Laboratory Director's Fund, Air Force Cambridge Research Laboratories, and the National Aeronautics and Space Administration, Wallops Station.

REFERENCES

Atlas, D., 1959: Radar studies of meteorological "angel" echoes, J. Atmospheric Terrest. Phys., 15, 262-287.

Atlas, D., 1959a: Sub-horizon radar echoes by scatter propagation, J. Geophys. Res., 64, 1205-1218.

Atlas, D., 1960: Possible key to the dilemma of meteorological "angel" echoes, J. Meteorol., 17, 95-103.

Atlas, D., 1960a: Radar detection of the sea breeze, J. Meteor., 17, 244-258.

Atlas, D., 1964: Advances in radar meteorology, Advan. Geophys., 10, 317-478.

Atlas, D., 1965: Angels in focus, Rad. Sci. J. Res., NBS/USNC - URSI, 69D, No. 6, 871-875.

Atlas, D., and K. R. Hardy, 1966: Radar analysis of the clear atmosphere: angels. Proc. XV General Assembly of URSI, Munich, Germany, 5-15 Sept., 401-469.

Atlas, D., K. R. Hardy, and K. Naito, 1966: Optimizing the radar detection of clear-air turbulence. J. of Appl. Meteor., 5, 450-460.

Atlas, D., K. R. Hardy, and T. G. Konrad, 1966a: Radar detection of the tropopause and clear air turbulence. Proc. 12th Weather Radar Conf., Amer. Meteor. Soc., Boston, 279-284.

Atlas, D., K. R. Hardy, K. M. Glover, I. Katz, and T. G. Konrad, 1966b: Tropopause detected by radar. Science 153, 1110-1112.

Booker, H. G., and W. E. Gordon, 1950: Theory of radio scattering in the troposphere. Proc. I.R.E., 38, 401-412.

Borchardt, H., 1962: Wolkenbeobachtungen mit einem doppelwelligen Radargerät. Beit. Physik Atmosphäre 35, 43-68. See also Atlas (1964).

Brunt, D., 1951: Experimental cloud formation. Compendium of Meteorology, Amer. Met. Soc., Boston, 1255-1262.

Chernikov, A. A., 1966: Some new Soviet investigations of angel echoes. Proc. 12th Weather Radar Conf., Amer. Meteor. Soc., Boston, Mass., 291-292.

Crawford, A. B., 1949: Radar reflections in the lower atmosphere, Proc. IRE, 37, 404-405.

Fehlhaber, L., and J. Grosskopf, 1964: Untersuchung der Structure der Troposphare mit einem Vertikalradar, Nachrichtentechnische Zeitschrift, 17(10), 503-507. English Translation - AFCRL, Bedford, Mass., TG-242, March 1965.

Glover, K. M., and K. R. Hardy, 1966: Dot angels: insects and birds. Proc. 12th Weather Radar Conf., Amer. Meteor. Soc., Boston, 264-268.

Glover, K. M., K. R. Hardy, T. G. Konrad, W. N. Sullivan, and A. S. Michaels, 1966: Radar observations of insects in free flight. Science, 154, 967-972.

Hajovsky, R. G., A. P. Deam, and A. H. LaGrone, 1966: Radar reflections from insects in the lower atmosphere. IEEE Trans. on Antennas and Propagation, 14, 224-227.

Hardy, K. R., and K. M. Glover, 1966: 24-hour history of radar angel activity at three wavelengths. Proc. 12th Weather Radar Conf., Boston, Mass., 269-274

Hardy, K. R., D. Atlas, and K. M. Glover, 1966: Multiwavelength backscatter from the clear atmosphere. J. Geophys. Res., 71, 1537-1552.

Haurwitz, B., 1941: Dynamic Meteorology, McGraw-Hill Book Co., Inc., New York.

Hay, D. R., and W. M. Reid, 1962: Radar angels in the lower troposphere, Can. J Phys., 40, 128-138.

Hicks, J. J., I. Katz, C. R. Landry, and K. R. Hardy, 1967: Simultaneous radar and aircraft observations of clear-air turbulence, Science, 157, 808-809.

Hicks, J. J., and J. K. Angell, 1968: Radar observations of breaking gravitational waves in the visually clear atmosphere. J. Appl. Meteor., 7, 114-121.

Konrad, T. G., and J. Hicks, 1966: Tracking of known bird species by radar. Proc. 12th Weather Radar Conf., Amer. Meteor. Soc., Boston, Mass., 259-263.

Konrad, T. G., and D. Randall, 1966: Simultaneous probing of the atmosphere by radar and meteorological sensors. Proc. 12th Weather Radar Conf., Amer. Meteor. Soc., Boston, 300-305.

Kropfli, R. A., I. Katz, T. G. Konrad, and E. B. Dobson, 1968: Simultaneous radar reflectivity measurements and refractive index spectra in the clear atmosphere. Proc. 13th Radar Meteorology Conf., Montreal, Canada.

Lane, J. A., 1964: Small-scale irregularities of the radio refractive index of the troposphere. Nature, 204, 438-440.

Lane, J. A., 1967: Radar echoes from tropospheric layers by incoherent back-scatter. Electronic Letters, 3, 173-174.

Ottersten, H., 1964: Occurrence and characteristics of radar angels observed with a vertically-pointing pulse radar. Proc. 11th Weather Radar Conf., Amer. Meteor. Soc., Boston, 22-27.

Petrocchi, J. J., and W. H. Paulsen, 1966: Meteorological significance of vertical density profiles of clouds and precipitation obtained with the AN/TPQ-11 radar. Proc. 12th Weather Radar Conf., Amer. Meteor. Soc., Boston, 467-472.

Plank, V. G., 1956: A meteorological study of radar angels. Geophys. Res. Paper 52, 117 pp., Air Force Cambridge Research Laboratories, Bedford, Mass.

Reiter, E. R., and A. Burns, 1966: The structure of clear-air turbulence derived from "TOPCAT" aircraft measurements. J. Atmos. Sci., 23, 206-212.

Saxton, J. A., J. A. Lane, R. W. Meadows, and P. A. Mathews, 1964: Layer structure of the troposphere - simultaneous radar and microwave refractometer investigations, Proc. I.E.E.E., 3, 275-283.

Tatarski, V. I., 1961: Wave propagation in a turbulent medium. McGraw-Hill Book Co., Inc., New York, N. Y., 285 pp.

Villars, F., and V. F. Weisskopf, 1954: The scattering of electromagnetic waves by turbulent atmospheric fluctuations, Phy. Rev., 94, 232-240.

Vrana, N., 1961: Some characteristics of radar angel echoes. Center for Radiophysics and Space Research, Res. Rept. No. 32, 29 pp., Cornell University, Ithaca, New York.